Phantom Materials for Elastography

Timothy J. Hall, *Member, IEEE*, Mehmet Bilgen, Michael F. Insana, *Member, IEEE*, and Thomas A. Krouskop

***Abstract*—Acoustic and mechanical properties are reported for gelatin materials used to construct tissue-like phantoms for elasticity imaging (elastography). A device and procedure for measuring elastic properties are described. The measured compression forces were comparable to results obtained from finite element analysis when linear elastic media are assumed. Also measured were the stress relaxation, temporal stability, and melting point of the materials. Aldehyde concentration was used to increase the stiffness of the gelatin by controlling the amount of collagen cross-linking. A broad range of tissue-like elastic properties was achieved with these materials, although gels continued to stiffen for several weeks. The precision for elastic modulus measurements ranged from less than 0.1% for 100 kPa samples to 8.9% for soft (< 10 kPa), sticky samples.**

I. Introduction

While all medical imaging modalities benefit from the availability of tissue-mimicking phantoms during their development, phantoms are essential to elastic imaging investigations. For example, to maximize the visibility of structures in a strain image, precise knowledge is required of the deformation a tissue undergoes when subjected to the stress and strain fields of a mechanical stimulus. Movement of scatterers out of the image plane, within the pulse volume, or any time-varying distortion of echoes in the range gate significantly reduces the signal-to-noise ratio for acoustic strain estimates [1]. Phantoms that mimic both acoustic and elastic properties of soft biological tissues under compression aid the development of effective data acquisition strategies and assessment of task performance.

The technology for manufacturing materials with tissue-like acoustic properties is well developed [2]–[5]. The essential requirements are mass density near 1.0 g/cm^3, sound speed near 1540 m/s, frequency-dependent attenuation coefficient near 0.5 dB/cm/MHz, and backscatter coefficient in the range of 10^{-5} and 10^{-2} between 2 MHz and 7 MHz that increases with frequency. Furthermore, the acoustic properties should be stable with time and temperature and adjustable to provide contrast. Water-based gels (hydrogels) developed by Madsen *et al.* [3]–[5] are the most successful ultrasonically tissue-mimicking materials that are fully disclosed in the literature, and are the subject of the present investigation.

The elastic properties of gels can also be found in the literature ([6], [7]). The elastic compressive properties of many biological tissues, such as breast and prostate, are not as well known, unfortunately (although Sarvazyan *et al.* [8] estimates the Young's modulus of soft tissues to range from 1 kPa to more than 1 MPa). Preliminary results reported by Parker *et al.* [9] have shown mixtures of agar and gelatin to lie in this range. Measurements for the tensile properties of muscle, blood vessels, some connective tissues, and skin are available [10]. Generally soft tissues behave as nonlinear viscoelastic solids. However, at rapid strain rates (faster than 0.5/sec) the behavior may be approximated as elastic and for narrow ranges of strain the modulus can be considered constant.

Measurements of the compression storage modulus (referred to here as Young's modulus) and stress relaxation function for hydrogels are presented below. Results show that the complexity of the constitutive equations required to describe forces and deformations depends on the experimental design.

Currently a strain image in static acoustic elastography is formed by comparing echo signals obtained prior to and immediately following less than 5% compression, where tissue properties are approximately linear and elastic. Under these conditions, the Young's modulus sufficiently characterizes the elastic response to compression. However, as signal processing methods for elastic imaging advance, larger strains are being attempted [11] and phantom materials may eventually need to mimic a fuller range of mechanical features.

The most useful phantoms are those that isolate individual features of an elastogram for study. For example, consider a long, cylindrically-shaped, hard inclusion placed in a uniformly soft background that undergoes uniaxial compression in a plane perpendicular to the cylinder axis. This phantom approximates a 2-D plane-strain state, and is used to study strain estimates where all the movement is in the image plane. It is simple in design, yet realistic in terms of features to be investigated, and can be modeled using most finite-element analyses. Contrast in this strain image is determined by the stiffness of the material [12]. Stiffness depends on the elastic modulus, the geometry of the sample being tested [13], and how the sample is constrained (boundary conditions). That is, strain images display elastic properties of materials in the context of their local environment. Uniaxial compression of inhomogeneous media generates nonuniform stress fields that create unusual strain patterns or "artifacts". Strain "artifacts"

Manuscript received December 17, 1996; accepted May 6, 1997. We gratefully acknowledge the support of NIH grant number PO1 CA64597 (University of Texas).

T. J. Hall, M. Bilgen, and M. F. Insana are with the University of Kansas Medical Center, Kansas City, KS 66160-7234 (e-mail: hall@research.kumc.edu).

T. A. Krouskop is with the Baylor College of Medicine, Houston, TX.

can be reduced by substituting the stress and strain fields into the constitutive equations to compute elastic modulus images [14]. So it is critical that phantom inclusions mimic tumors and other objects with respect to their representative shape, size, and placement in the stress and acoustic fields. The elastic properties of phantom components should be chemically stable to prevent changes in contrast over time. Hydrogels possess many of the most important features necessary for building elastographic phantoms.

II. Materials and Methods

A. Materials

Although hydrogels are the focus of this work we have considered numerous alternatives. Among the alternatives were various polymer gels, and silicone gels. However, as reported by Madsen *et al.* [3], [4], these materials either possess sound speeds that are substantially less than 1500 m/s or their attenuation is too high (typically greater than 2 dB/cm/MHz and nonlinear with ultrasonic frequency) which makes them unsuitable for sonography and elastography phantoms. A notable exception is the acrylic polymer reported by Zerhouni and Rachendine [15].

Manufacturing methods are the key to controlling sonographic and elastographic properties of the resulting phantom materials. As previously described [2]–[4] gel powder (either agar or animal hide) is hydrated with a solution of deionized water and *n*-propanol and heated above its gel point (35 to 40°C for animal hide gelatins) to disperse the colloid, clarify the solution, and release trapped gasses. *N*-propanol is added to the water to increase sound speed. While the gel solution is liquid, graphite flakes and glass beads can be added to increase the absorption and scattering. The mixture is rotated about 1 rpm to prevent settling of the glass and graphite while the gel congeals. Gelation (cross-linking among collagen fibers) occurs when the mixture is sufficiently cold (approximately 26°C for gelatin). Producing high-quality, tissue-mimicking phantom materials for elastography requires these techniques plus the additional control over the temperature and the time during which the colloid is dispersed. Animal hide gels hydrolyze, which reduces the ultimate gel strength, when held at elevated temperatures for an extended period of time [16]. Therefore, we modified the above procedure by placing hydrated gelatin in a vacuum (26 to 28 in Hg) to degas the solution thus reducing the heating time and temperature required to disperse the colloid and clarify the solution. A homogeneous gel is produced by raising the temperature of the solution to 45°C in a constant-temperature water bath. Graphite and/or glass beads are added at that time to obtain the desired scattering and absorption properties. The mixture is then cooled to 30°C (near its congealing point) in an ice water bath, and a small quantity of formaldehyde or other hardener is added to increase cross-linking and thus raise the melting point of the congealed gel. The mixture is then poured into the phantom container and rotated until it has congealed. The resulting gels are thought to be a homogeneous, isotropic, dense network of filaments [17].

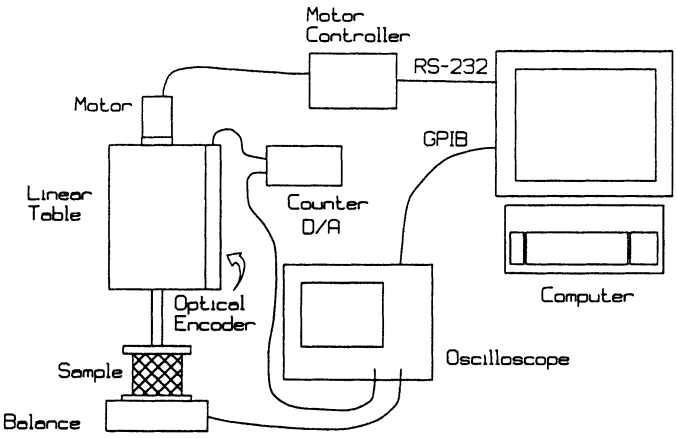

Fig. 1. An illustration of the experimental apparatus used to measure Young's modulus of gel samples. The sample is compressed under computer control, and the time-dependent force and position signals, Fig. 2, are digitized and stored off-line for stress-strain analysis.

B. Measurement Methods

We developed an apparatus to measure the mechanical properties of the test materials. A sketch of the apparatus (Fig. 1) shows key elements of its design. A linear table, equipped with a computer-controlled stepper motor and an optical encoder, is mounted vertically in a rigid, massive framework. A compressor that is larger than the sample surface is mounted to the linear table and is moved by the stepper motor. The quadrature signals from the encoder are converted to an analog voltage proportional to the vertical position of the compressor. The sample to be tested is placed on the tray of a standard electronic balance. The balance has been modified to provide a voltage proportional to the force on the balance. The stepper motor system is used to first uniaxially preload the sample, and then sinusoidally load and unload the sample at a fixed frequency (0.4 Hz in this study) for a specified number of cycles. The time-dependent position and force signals are digitized and stored with a digital oscilloscope. When properly scaled (see Data Analysis subsection below) these signals provide strain and stress estimates as a function of time, as shown in Fig. 2. All samples included in this study were cylinders 5.4 cm in diameter, 5.0 cm long unless otherwise noted. Typically, samples were preloaded to 4% strain (2 mm) and then compressed an additional 10% (5 mm). All measurements were performed at room temperature (20 to 21°C).

C. Data Analysis

The data shown in Fig. 2 provide the information necessary to characterize the mechanical properties of a phantom material for elastography. The amplitude of the force versus time curve shows that the force required to com-

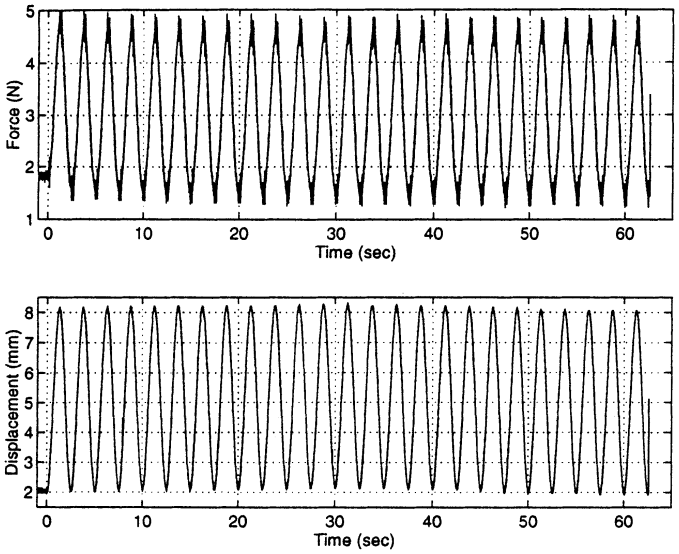

Fig. 2. Plots of the force versus time and displacement versus time for a 78 mm diameter soft gelatin sample.

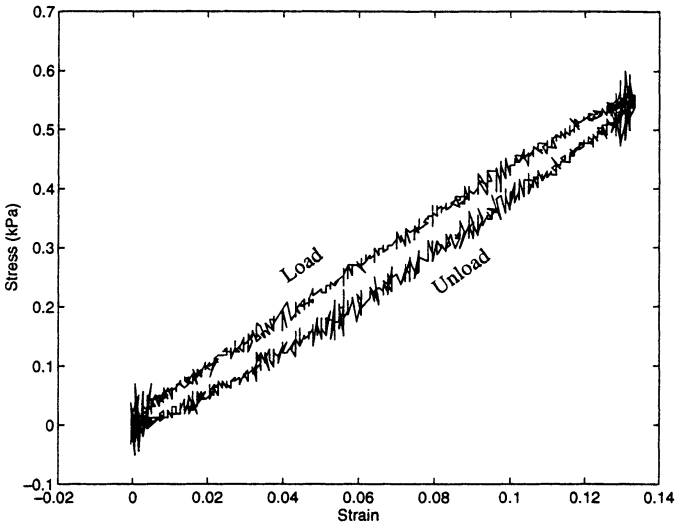

Fig. 3. A plot of the stress versus strain from the 24th cycle of the data in Fig. 2. The Young's modulus for this sample, estimated from the slope of this curve, is approximately 4.1 kPa.

press the sample a given amount decreases initially before becoming quite stable, a phenomenon referred to as preconditioning [10]. There is, typically, less than a 1° phase difference between the compressor displacement curve and the force curve on loading and a 0 to 6° phase difference on unloading. Therefore, as suggested by Fung [18], we chose to model these materials as linear elastic materials for the load portion of the curve, and as viscoelastic materials for the unloading portion. With the assumption of linear elasticity, Young's modulus equals the slope of the load portion of the stress-strain curve where stress σ and strain e are defined as follows [19]:

$$\sigma = \frac{F(t)}{A(t)} \tag{1}$$

$$e = -\int_{h_0}^{h(t)} \frac{dh}{h} \tag{2}$$

where $F(t)$ is the force, $A(t)$ is the sample area, $h(t)$ is the sample height at time t, and h_0 is the height following preloading. If the sample is allowed to freely slip at its boundaries, there is uniform displacement of the surfaces perpendicular to the compressed surface, and the estimated modulus is a good estimate of the true Young's modulus of the material. We selected a single cycle of the stress and strain curves, following at least 20 cycles for preconditioning, to estimate Young's modulus for these materials, as shown in Fig. 3. Note that "true" definitions for stress and strain, those that include instantaneous sample height and diameter, are used in this work as suggested in the ASTM standard for measurements of Young's modulus in metals [20] when strains exceed 0.25%. The uncertainty in stress and strain and the resulting uncertainty in Young's modulus is discussed in the Results section.

No reference standard materials are available for calibration of this equipment in this stiffness range. Therefore, the accuracy of these measurements is difficult to judge. However, our measurements were in agreement with predictions from finite element analysis, as described in the Results section.

III. Results

A. Measurement Precision

Three sets of five samples (sets A, B, and C, see Table I) were manufactured to study the precision of Young's modulus measurements. All five samples within each set were manufactured at the same time from the same colloid solution. Comparison of values within a set of samples addresses measurement precision and not manufacturing reproducibility since inter-batch variability is likely much larger than intra-batch variability.

The uncertainty at a point on the stress-strain curve can be estimated by propagating experimental uncertainties (± 200 μm uncertainty in sample height, ± 1 μm position uncertainty, 20 mV peak-peak electronic noise, and 8-bit sampling) and those results used to determine the uncertainty in the slope of the stress-strain curve [21]. Fractional uncertainties in stress and strain are approximately 1.2% and 1.7%, respectively, at the lowest points on the stress-strain curve (minimum voltage) with fractional uncertainties diminishing as the stress and strain (voltages) increase. Uncertainty in the slope of the stress-strain curve for a single measurement of an individual sample range from approximately 1.8% for soft (< 10 kPa), sticky samples to 0.1% for 100 kPa samples.

Sample set A was a relatively stiff gel. Young's modulus measurements were made over a 246-day period for this set and are shown in Fig. 4. The standard deviation among modulus estimates for the five samples was typically less than 1%. To verify that the measurement proce-

TABLE I
DESCRIPTION OF THE GEL SAMPLES USED IN THIS STUDY.*

Set	Number	Gelatin Type	Gel	*n*-propanol	Water	Hardener	Graphite
A	1–5	A—275 Bloom‡	120	80.2	900	4.33 (F)	0
B	1–5	B—100 Bloom	120	80.2	900	0.133 (P)	50
C	1–5	B—100 Bloom	120	80.2	900	0.133 (P)	0
D	1–10	Agar	5–30	80.2	900	0	0
E	1–10	A—275 Bloom	30–180	80.2	900	4.33 (F)	0
F	1–5	A—275 Bloom	90	40.1	950	0.100–4.00 (F)	50
G	1–5	A—275 Bloom	90	40.1	950	1.15–28.67 (P)	50

* The mass of each gel component is given in grams. The hardeners were either formaldehyde (F) or paraformaldehyde (P). Gelatin powder was obtained from Vyse Gelatin Company. Agar, *n*-propanol, formaldehyde, paraformaldehyde, and graphite were obtained from Fisher Scientific. The weight for formaldehyde was that of a 37.3% solution.

‡Bloom strength is a measure of the rigidity of a gel formed under prescribed conditions, and is the official procedure of the Gelatin Manufacturers Institute of America, Inc., 1986.

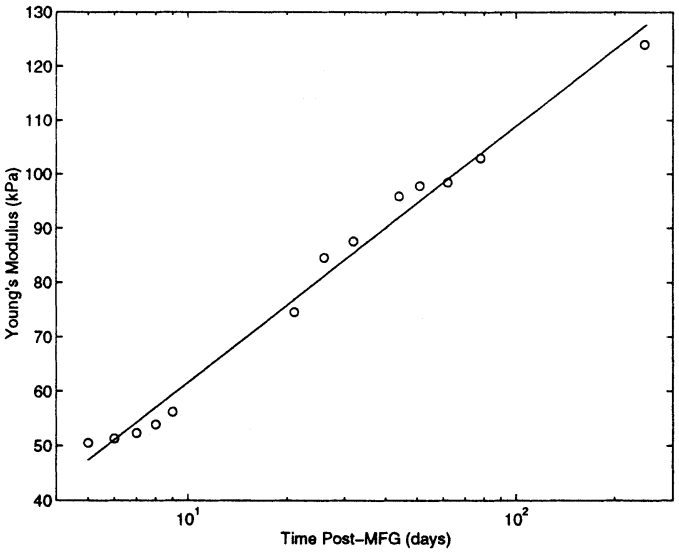

Fig. 4. A plot of the average Young's modulus versus time for a set of five identical samples. Standard errors among measurements at a given time were less than 0.1% (not visible on this plot). The solid line is a least squares fit to the data.

dure was not stiffening these samples, we measured two of the samples five times on two occasions. No statistically significant differences were found between those samples measured once per study and those measured five times per study. The stiffness versus time has a functional form similar to that found by Djabourov *et al.* [17] who studied the kinetics of gel formation for 1,000 hours by measuring the optical rotation as an indication of gelation.

Sample sets B and C were relatively soft samples that were manufactured at the same time and were identical in composition, except that set B contained large graphite flakes added for ultrasonic absorption and scattering. The results of these measurements, shown in Table II, suggest that graphite at this concentration produces a small effect on gel stiffness. These results also indicate that the standard deviation among a set of measurements for softer samples is higher, but is still only $\sim 5\%$ on average. The loss in estimated Young's modulus over time is likely due

TABLE II
RESULTS OF ESTIMATES OF YOUNG'S MODULUS FOR TWO SETS OF FIVE IDENTICAL SAMPLES OVER A 52-DAY PERIOD SHOWING THE AVERAGE VALUES AND THE STANDARD ERROR.

Time	A	vg. E (kPa)
Post-MFG (d)	no graphite	with graphite
17	6.18 ± 0.55	7.66 ± 0.12
23	5.09 ± 0.13	5.95 ± 0.27
35	4.40 ± 0.30	6.07 ± 0.51
42	5.03 ± 0.07	5.44 ± 0.22
52	5.28 ± 0.19	5.70 ± 0.17

to an error in estimating the sample diameter for stress calculations. Creep caused these samples to lose 20% of their original height over the 52-day measurement period. Although this distortion in shape was nonlinear with height, we assumed constant sample volume and cylindrical shape, and estimated the sample diameter from the measured sample height. Stiffer samples did not suffer this extensive creep.

B. Gel Composition and Stiffness

Sample sets D and E were made to study the effects of powdered gel concentration on the stiffness of the congealed gel. Set D was manufactured with agar concentrations ranging from 5.0 g/L to 30.0 g/L of *n*-propanol in water by heating a large quantity of agar solution (30.0 g/L) and thinning it to the desired concentration with heated *n*-propanol solution. Similarly, set E was manufactured from gelatin with concentrations ranging from 30.0 g/L to 180.0 g/L. In this case the colloid was dispersed by heating the solution to 85°C for 1 to 2 hours which likely resulted in a 15 to 20% loss in stiffness [16]. The results of measurements on these samples are shown in Figs. 5 and 6, respectively. Young's modulus (E in kPa) was roughly proportional to the square of the gel concentra-

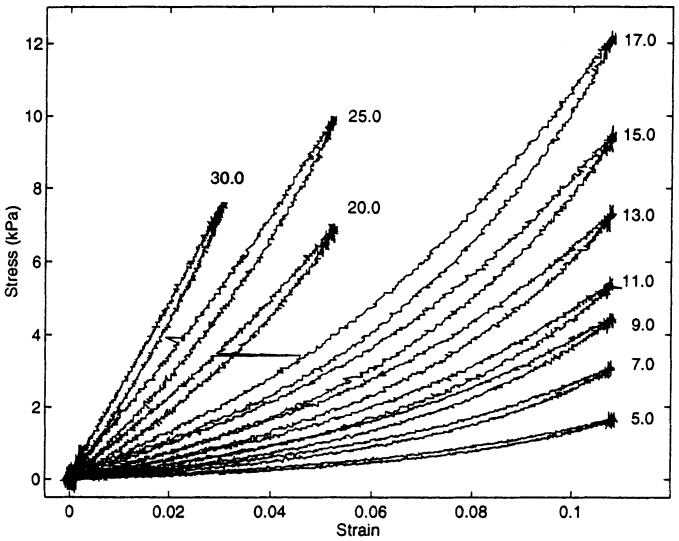

Fig. 5. A plot of the stress versus strain as a function of agar concentration. Concentrations ranging from 5.0 g/L to 30.0 g/L resulted in Young's moduli ranging from 7.6 kPa to 195 kPa, respectively (for small (0 to 2%), approximately linear stresses).

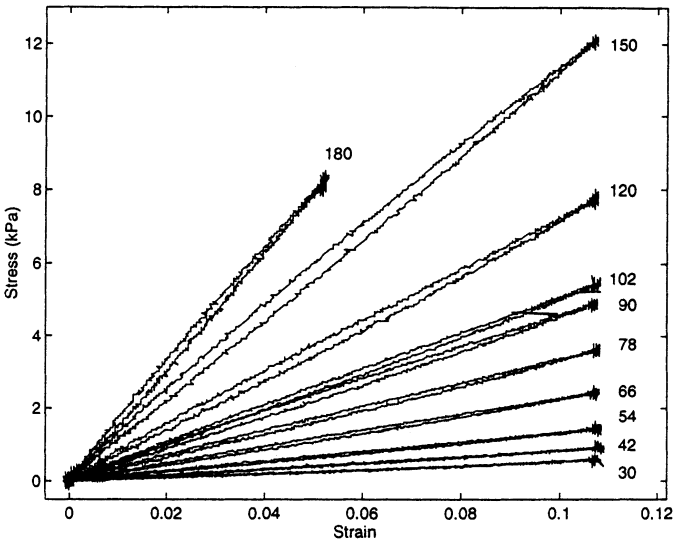

Fig. 6. A plot of the stress versus strain as a function of gelatin concentration. Concentrations ranging from 30.0 g/L to 180.0 g/L resulted in Young's moduli ranging from 4.8 kPa to 158 kPa, respectively.

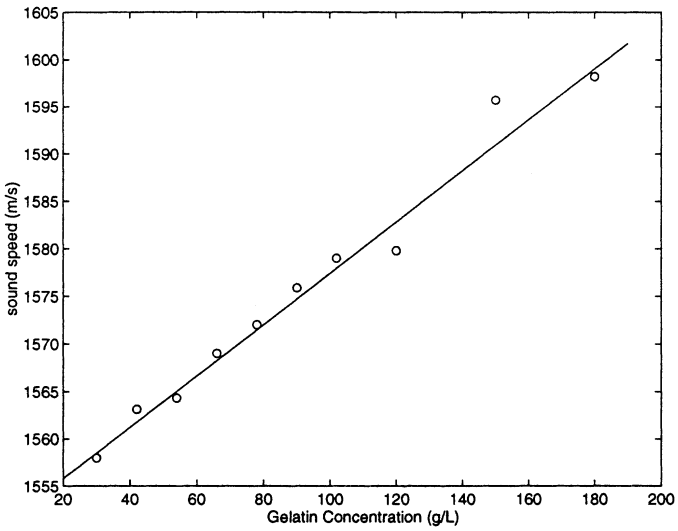

Fig. 7. A plot of the sound speed as a function of gelatin concentration. For concentrations (C) ranging from 30 g/L to 180 g/L sound speed $= 1550.4 + 0.275{*}C$.

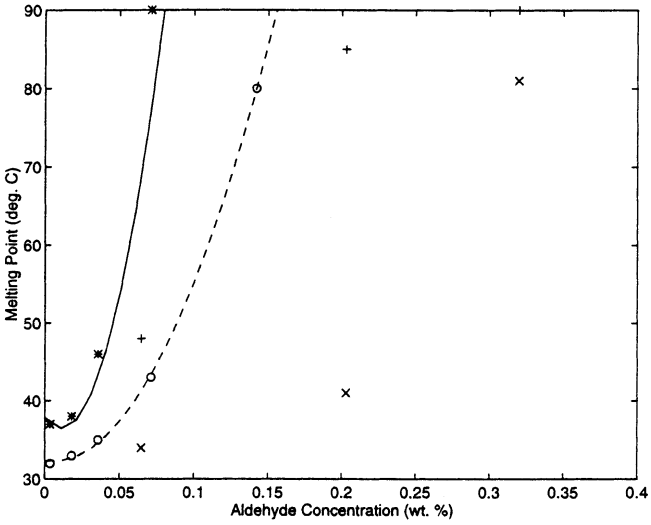

Fig. 8. A plot of the melting point for gelatin samples as a function of formaldehyde (o,*) and paraformaldehyde (x,+) concentrations measured 7 (dashed line, o, x) and 19 days (solid line, *, +) post-manufacture. The lines are the least-squares fits for formaldehyde samples.

tion (C in g/L),

$$E_{\text{agar}} = 0.349C^{1.87} \quad (r = 0.999) \text{ and} \tag{3}$$

$$E_{\text{gelatin}} = 0.0034C^{2.09} \quad (r = 0.997) \tag{4}$$

in agreement with that reported by Ferry [6] and many others. In addition, sound speed in the congealed gelatin was found, via through-transmission measurements [4], to increase linearly with gelatin concentration, as shown in Fig. 7.

Aldehydes can be used to increase the cross-linking in gelatin gels and thus raise the melting point [7]. To study the effects of aldehyde concentration on gel properties, we manufactured sample sets F and G which had a fixed concentration of gelatin, water, *n*-propanol, and graphite, but varying hardener concentrations, as shown in Table I. Formaldehyde was added to set F at concentrations from 0.0036 to 0.14 (wt.%). Similarly, paraformaldehyde was added to set G at concentrations from 0.065 to 2.5. Melting points were estimated by placing a small portion of each sample in a beaker of water and raising the temperature approximately 0.2°C/min in a constant temperature bath until the sample lost structural form. Melting points were measured at 7 and 19 days post-manufacture. Melting points of these two sets of samples are shown in Fig. 8. Formaldehyde raises the melting point of gelatin faster than paraformaldehyde at equal concentrations. Formaldehyde concentrations in excess of 0.08% produce gels that

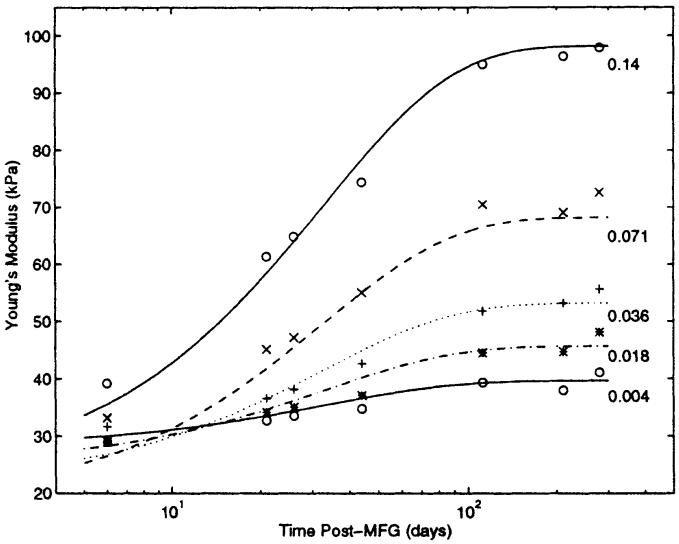

Fig. 9. A plot of Young's moduli as a function of time for gelatin samples with formaldehyde concentrations (wt.%) ranging from 0.0036 to 0.14. Increasing formaldehyde concentration greatly increases gel stiffness.

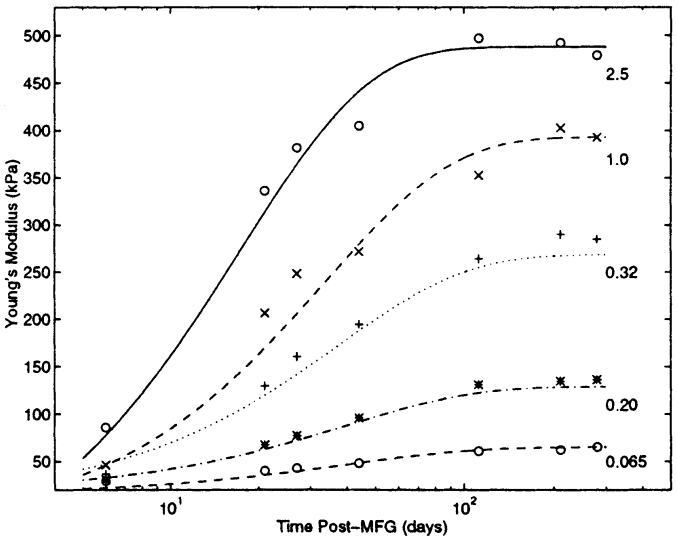

Fig. 10. A plot of Young's moduli as a function of time for gelatin samples with paraformaldehyde concentrations (wt.%) ranging from 0.065 to 2.5. Increasing paraformaldehyde concentration greatly increases gel stiffness.

are stable at elevated room temperatures within 7 days. Within 3 weeks post-manufacture, the melting point is higher than 65°C. Results of Young's modulus measurements on these samples over a 211 day period are given in Figs. 9 and 10, respectively. The Young's modulus (E) was modeled as a function of time (t, days) and aldehyde concentration (C, g/L) for these samples and found to be well represented by the expression

$$E = Y_1 - Y_2 \exp(-t/33) \tag{5a}$$

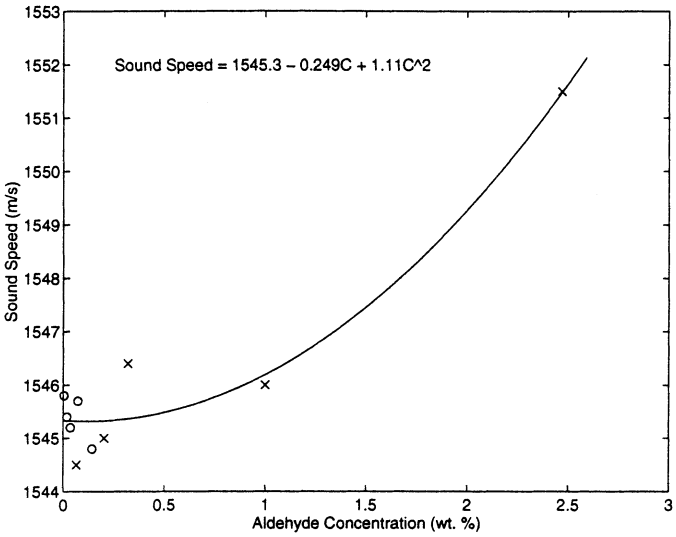

Fig. 11. A plot of sound speed in gelatin samples as a function of formaldehyde (o) and paraformaldehyde (x) concentration. The solid line is the least-squares fit of the combined data.

where

$$Y_1 = 38.1 + 382C \tag{5b}$$

$$Y_2 = 9.1 + 617C - 1255C^2 \tag{5c}$$

for the formaldehyde samples and

$$E = Y_1 - Y_2 \exp(-t/T) \tag{6a}$$

where

$$Y_1 = 500 - 510 \exp(-1.45C) \tag{6b}$$

$$Y_2 = 620 - 640 \exp(-1.05C) \tag{6c}$$

and

$$T = 53 - 12 \exp(C/2.4) \tag{6d}$$

for the paraformaldehyde samples. These equations are plotted along with the measured data in Figs. 9 and 10. Sound speed for these samples are shown in Fig 11. The scattering and attenuation properties of these samples were observed qualitatively by simultaneously scanning pairs of samples with a 5 MHz linear array imaging system (Siemens Q2000) under identical conditions. No differences were observed in the scattering or attenuation properties among these samples. Therefore, aldehyde concentration has little or no effect on backscatter coefficients and attenuation coefficients, or on sound speed for concentrations below about 1%.

In some cases the sample was too stiff to compress to 4% preload and an additional 10% for modulus estimation, e.g., Figs. 5 and 6. For these samples, the use of a compressor smaller than the sample surface area was suggested. To study the effects of using a smaller compressor, we made a sample with a Young's modulus of approximately 46 kPa

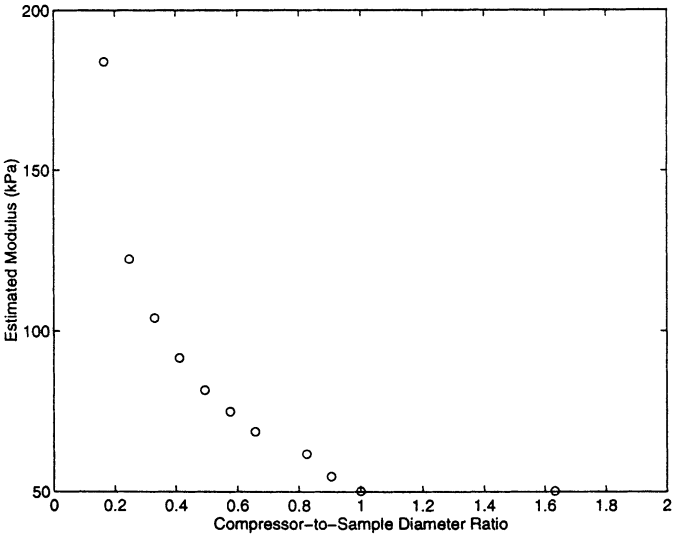

Fig. 12. A plot of the estimated elastic moduli as a function of compressor diameter for a gelatin sample 7.6 cm diameter and 2.5 cm thick with Young's modulus of 46 kPa.

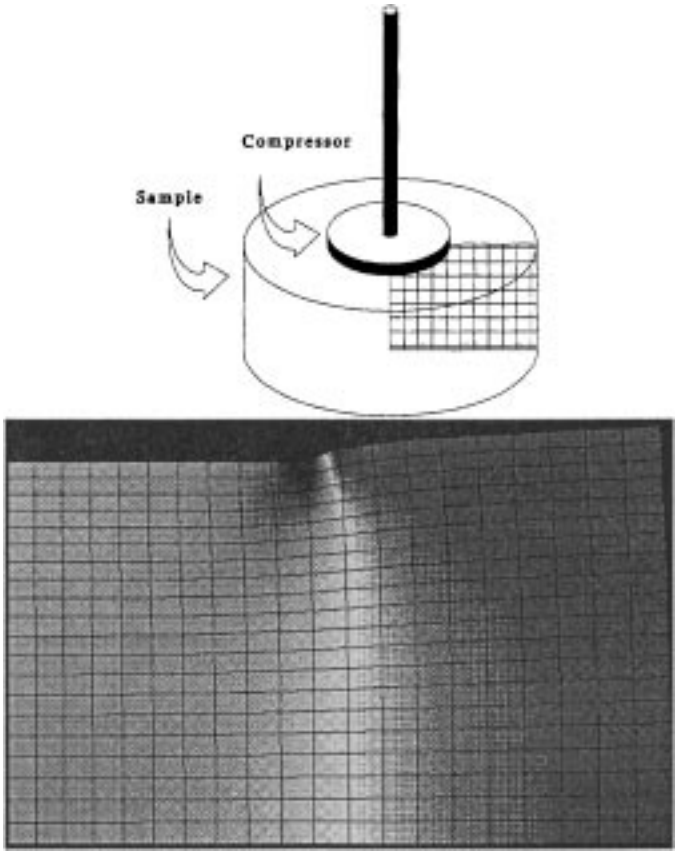

Fig. 13. An axial stress distribution from a FEA simulation showing the effects of compressing the top of a sample with a compressor smaller than the sample surface area. The compression is not uniaxial, as required to estimate Young's modulus.

that was 7.6 cm diameter and 2.5 cm thick. We then compressed that sample with flat circular compressors ranging in diameter from 1.27 to 12.55 cm. If we define stress as the force per unit area of the compressor (for compressors smaller than the sample) and define strain as the fractional displacement of the compressor, we obtain elastic modulus estimates that are biased increasingly high with decreasing compressor diameters, as shown in Fig. 12. To understand this bias and how other experimental conditions affect the measurement, we employed finite element analysis (FEA), as described below. A simple illustration of the problem with this definition of stress is shown in Fig. 13.

C. Examining Boundary Conditions

FEA was used to model our experimental procedures to understand the importance of boundary conditions. A commercial software package (ALGOR, Inc., Pittsburgh, PA) was used in this work. A linear stress analysis was performed in 3D using axial symmetry.

A uniform displacement of 10% was used to model the force at the base of the sample from compressors of various sizes. We examined two sets of boundary conditions: one where the sample was free to slide radially at its surfaces (unbound) and another where the sample was bound at the surfaces of both top and bottom compressors. The stresses in each case were integrated over the bottom surface of the sample and the resulting modeled force compared with the measured force from phantom experiments. This procedure was repeated for two values of Young's modulus (46 kPa and 2.5 kPa), and the results are shown in Fig. 14.

The measured forces for the 46 kPa sample agree very well with the unbound condition suggesting that the conditions for this experiment were approximately those required to obtain true Young's modulus estimates when the compressor is at least as large as the sample. We can assess the accuracy of our Young's modulus estimates by comparing the measured forces with the FEA calculated forces. If we assume the measured Young's modulus of 46 kPa is correct, the measured forces are, on average, 7.5% high. From this it is reasonable to assume that, if we are able to achieve free slip boundary conditions, our measured Young's modulus is accurate within about 8%.

The FEA results for a 2.5 kPa sample bound at its surfaces agree very well with our measured forces for a sample for which we estimated Young's modulus to be 5.8 kPa. Thus, our estimate of Young's modulus in this sample is biased high due to the apparent fact that the sample was not freely sliding radially as it was being compressed axially. FEA results suggest that partially bound surfaces can cause as much as a 234% overestimate in Young's modulus.

Those results, which were for a specific sample geometry, were generalized by using FEA to model the force obtained under unbound conditions for samples of various thicknesses and diameters with Poisson's ratio of 0.495. The results, shown in Fig. 15 for a 7.62 cm diameter sample, show that the force generated at 10% strain depends on the compressor-to-sample diameter ratio and the sample thickness-to-diameter ratio. These results are general in that they can be scaled to any diameter (for the thick-

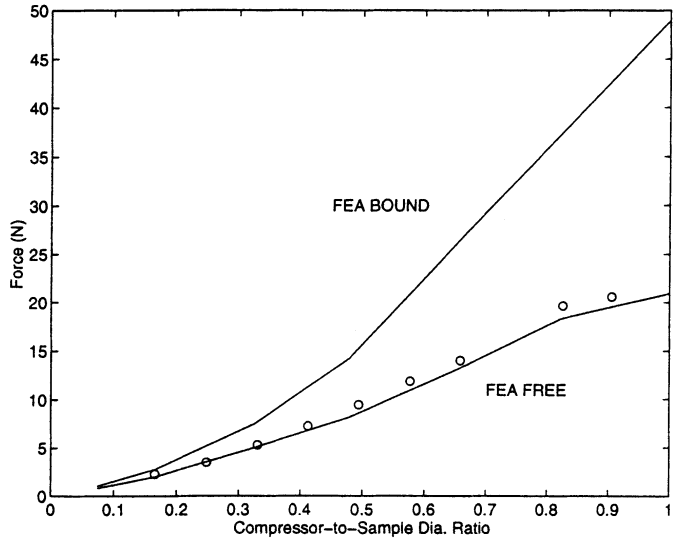

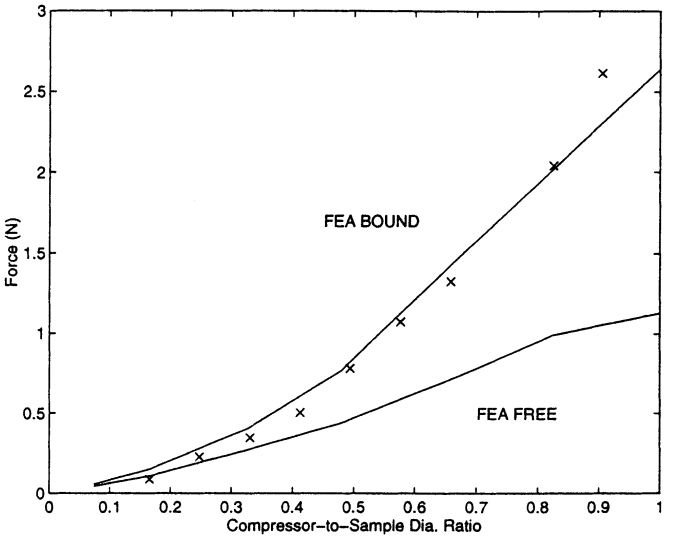

Fig. 14. Results of a FEA simulation to estimate the net force at the base of a sample. The top of a sample was displaced with a compressor smaller than the sample surface area. The sample was either free to slide across the compressor surfaces or bound to the compressor surfaces. Measurements on a 46 kPa sample (o) suggest that the sample slid freely, while measurements on a 2.5 kPa sample (x) suggests the surfaces are bound to the compressor surface. The 2.5 kPa sample was sticky to touch, even though it was lubricated with oil for measurements. In the bound case the compression is not uniaxial, as required to estimate Young's modulus.

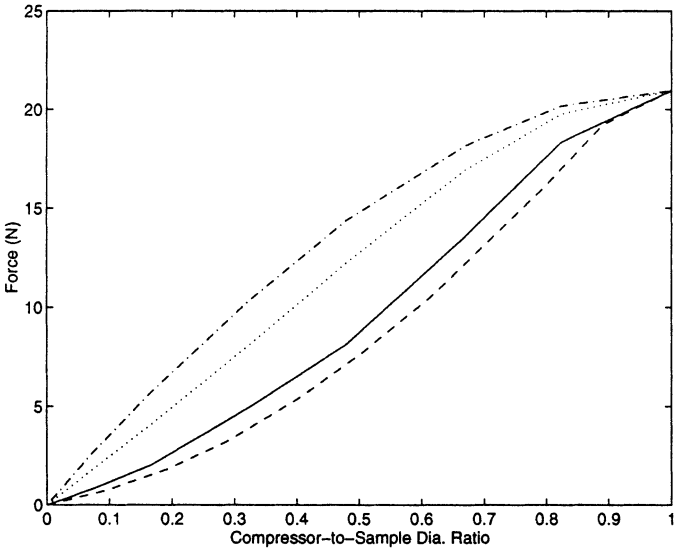

Fig. 15. FEA simulation results of the net force versus compressor size. The 7.62 cm diameter 46 kPa sample is examined for the free-slip boundary conditions. Results are shown for sample height-to-diameter ratios of 0.2 (dashed), 0.33 (solid), 0.67 (dot), and 1.00 (dot-dash). Forces scale with sample area and with Young's modulus, assuming linear elastic media.

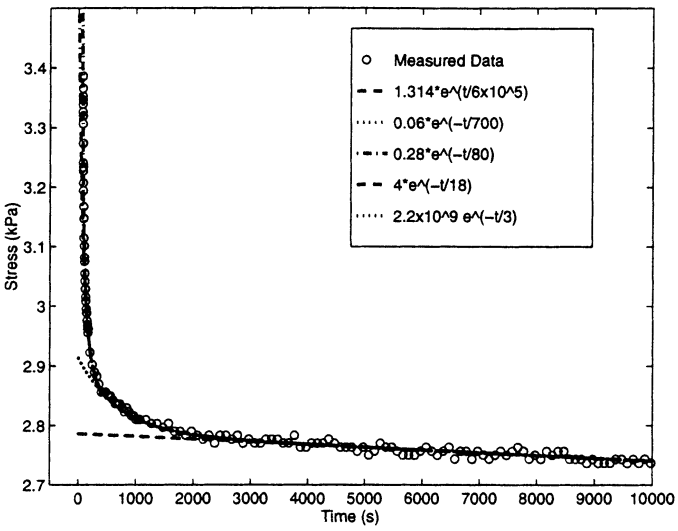

Fig. 16. Results of a stress relaxation experiment on a gelatin sample.

ness ratios shown) and any Young's modulus values (assuming linear elastic media). The measurements were repeated assuming Poisson's ratios of 0.490 and 0.498 and results were found to differ by less than 0.5%.

The viscoelasticity of gels was also investigated using a stress relaxation experiment. A 7.6 cm diameter 2.5 cm thick sample with $E = 55$ kPa was compressed to 5% strain in 0.1 s and held in this compressed state. The stress was measured continuously for 10,000 s (2.8 hours). The stress decay was accurately modeled as the sum of five decaying exponentials with time constants of 3, 18, 80, 700, and 600,000 seconds, as shown in Fig. 16. Similar results were obtained with samples with $E = 22$ kPa and 126 kPa.

IV. Discussion

Gelatin gels exhibit a nearly linear stress-strain curve (for strains less than 10%, Fig. 6) and are, therefore, preferred over agar gels. Because agar gels exhibit nonlinear stress-strain behavior (Fig. 5), their stiffness depends on the preload and measurement conditions. Therefore, contrast in a phantom would depend on how the data were acquired, and measurements of image contrast would be difficult to reproduce.

The results above show that a broad range of Young's

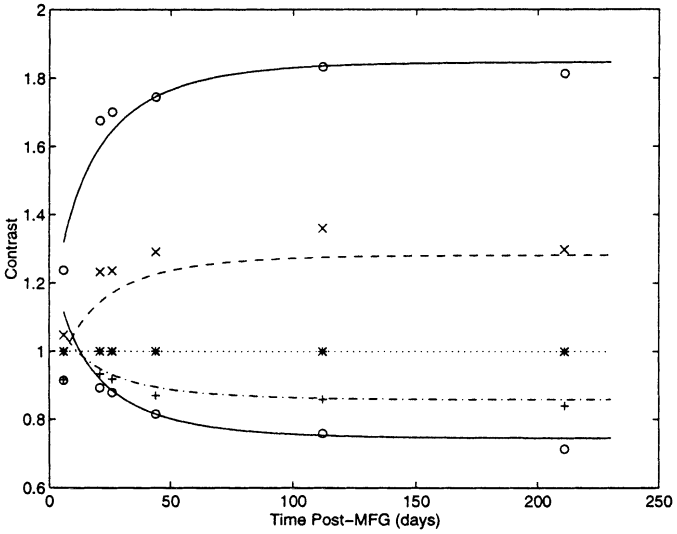

Fig. 17. Contrast as a function of time for phantom materials which include formaldehyde. Contrast was calculated as the ratio of Young's moduli, relative to the third member of the set (chosen arbitrarily). Data points are the ratio of measured values shown in Fig. 9. The curves are the ratio of predicted values using (5a).

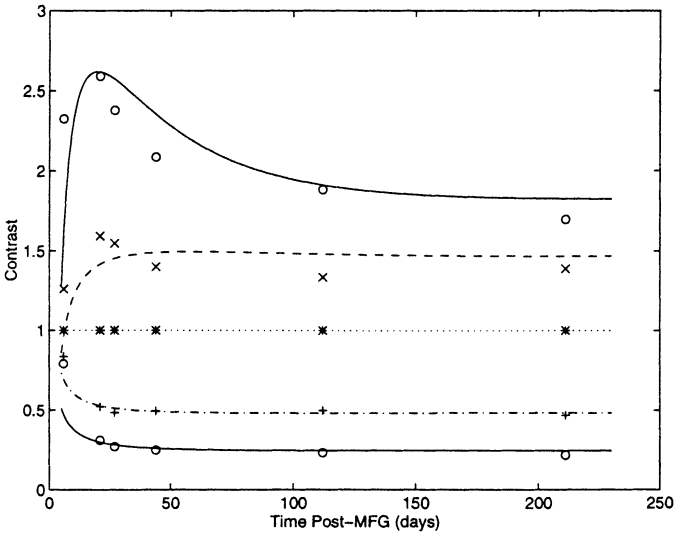

Fig. 18. Contrast as a function of time for phantom materials, which include paraformaldehyde. Contrast was calculated as the ratio of Young's moduli, relative to the third member of the set (chosen arbitrarily). Data points are the ratio of measured values shown in Fig. 10. The curves are the ratio of predicted values using (6a).

modulus values can be obtained by using gelatin for phantom materials. Some gel materials were too soft to maintain structural form, and we estimate their Young's moduli less than 2 kPa (2.5 kPa was the softest samples we could measure). An upper limit on gel stiffness was not obtained, but the range of Young's moduli obtained varies by more than a factor of 200. Therefore, most needs for tissue-mimicking phantom materials can be met by gelatin gels.

Although the stiffness of gelatin gels continues to increase over time (Figs. 9 and 10), (5) and (6) can be used to predict stiffness at a given time post-manufacturing. Figs. 17 and 18 show that the contrast in a phantom becomes relatively stable and, more importantly, predictable. In addition, Figs. 4, 9, and 10 suggest that the gels may be reaching an equilibrium condition, albeit more than 1000 hours post-manufacturing.

Although the Young's moduli produced in these materials varies by more than a factor of 200, this range may be difficult to produce in a composite phantom. When dissimilar materials are juxtaposed, osmotic forces cause fluid to migrate across the interface between different phantom materials. To minimize osmotic forces, the concentrations of phantom materials must be equal in the target and background. Although we have not investigated the severity of this problem for differing formaldehyde concentrations, it is reasonable to assume that juxtaposition is a smaller problem for faster cross-linking rates. Figs. 9 and 10 show that paraformaldehyde generates cross-links faster than formaldehyde.

The significant bias in the expected force of compression found with FEA for bound versus unbound conditions can cause significant errors in measurement results. Since it can be difficult to assure free-slip conditions, it may be best to attempt bound conditions and use the FEA results to scale the modulus estimates to true moduli.

Measurements were made at a single sinusoidal frequency and at room temperature. Each of these parameters might affect the viscoelastic properties of hydrogels. However, te Nijenhuis has shown [22] that the storage modulus is nearly frequency independent for cycling frequencies between 0.04 and 6 Hz for gelatin gels. The temperature dependence in the storage modulus near room temperature requires further investigation.

The measurement technique shown here is similar to that reported by Chen *et al.* [23]. Our methods differ in several ways. First, we used continuous estimation of stress and strain instead of step-wise measurements. All material characterization was done with compressors larger than the samples being studied; therefore, no corrections for compressor size were made in modulus estimation. FEA results are presented that demonstrate the effects of compressor size and sample thickness in making this correction. In addition, measurements of sample compression were made via an optical encoder; therefore, no assumption were necessary regarding the constancy of sound speeds when the sample is compressed.

The viscoelastic measurements show that significant stress relaxation occurs in gelatin samples during the first 15 minutes following an abrupt compression. Therefore, elasticity measurements must be made in a time frame on the order of 1 s or less (or greater than 10s of minutes) to avoid significant stress relaxation effects in modulus estimates. Thus, any step-wise compression schemes for elastographic imaging are likely to be perturbed by stress relaxation effects.

V. Conclusions

The use of water-based gels for elastography was investigated. Results show that gelatin gels can provide a wide range of stiffness approximating that of soft tissues. It is possible to independently control the gel stiffness, sound speed, absorption, and scattering. The use of aldehydes to increase the melting point of the gel simultaneously increases the stiffness in a predictable manner. Although the gels continue to stiffen over time, their stiffness appears to stabilize, and the rate of stiffening has been modeled. Therefore, contrast in a phantom is predictable and becomes relatively stable. Improved stability of phantom contrast is desirable. Further work is needed to obtain high quality reference materials.

Stress relaxation in these materials was also investigated. Results show that significant stress relaxation occurs during the first few minutes following an abrupt compression. These results suggest that stress relaxation is a likely source of echo signal decorrelation thus reducing the signal-to-noise ratio in elastographic imaging.

Acknowledgment

We are grateful to Brian Bailey who assisted in making some of the elastic modulus measurements at KUMC.

References

[1] M. Bilgen and M. F. Insana, "Error analysis in acoustic elastography: II. Strain estimation and SNR analysis," *J. Acoust. Soc. Amer.*, vol. 101, no. 2, pp. 1147–1156, 1997.

[2] T. J. Hall, M. F. Insana, N. M. Soller, and S. J. Rosenthal, "Ultrasound contrast–detail analysis: A preliminary study in human observer performance," *Med. Phys.*, vol. 20, pp. 117–127, 1993.

[3] E. L. Madsen, J. A. Zagzebski, R. A. Banjavic, and R. Jutila, "Tissue mimicking materials for ultrasound phantoms," *Med. Phys.*, vol. 5, pp. 391–394, 1978.

[4] E. L. Madsen, J. A. Zagzebski, and G. R. Frank, "Oil-in-gelatin dispersions for use as ultrasonically tissue-mimicking materials," *Ultrason. Med. Biol.*, vol. 8, no. 3, pp. 277–287, 1982.

[5] E. L. Madsen, "Ultrasonically soft tissue–mimicking materials and phantoms," in *Tissue Characterization with Ultrasound*, J. F. Greenleaf, Ed. Boca Raton, FL: CRC Press, 1986, pp. 165–181.

[6] J. D. Ferry, "Mechanical properties of substances of high molecular weight. IV. Rigidities of gelatin gels; dependence on concentration, temperature and molecular weight," *J. Amer. Chem. Soc.*, vol. 70, pp. 2244–2249, 1948.

[7] B. Tabor, "Crosslinking efficiency of gelatin hardeners," *J. Appl. Polym. Sci.*, vol. 12, pp. 1967–1979, 1968.

[8] A. Sarvazyan, A. Skovoroda, S. Emelianov, J. Fowlkes, J. Pipe, R. Adler, R. Buxton, and P. L. Carson, "Biophysical bases of elasticity imaging," in *Acoustical Imaging*, J. P. Jones, Ed. New York: Plenum, 1995, pp. 223–240.

[9] K. J. Parker, S. R. Huang, R. A. Musulin, and R. M. Lerner, "Tissue response to mechanical vibrations for sonoelasticity imaging," *Ultrason. Med. Biol.*, vol. 16, no. 3, pp. 241–246, 1990.

[10] Y. C. Fung, *Biomechanics: Mechanical Properties of Living Tissues*, 2nd ed. New York: Springer-Verlag, 1993.

[11] M. O'Donnell, A. R. Skovoroda, B. M. Shapo, and S. Emelianov, "Internal displacement and strain imaging using ultrasonic speckle tracking," *IEEE Trans. Ultrason., Ferroelect., Freq. Contr.*, vol. 41, no. 3, pp. 314–325, 1994.

[12] H. Ponnekanti, J. Ophir, Y. Huang, and I. Céspedes, "Fundamental mechanical limitations on the visualization of elasticity contrast in elastography," *Ultrason. Med. Biol.*, vol. 21, no. 4, pp. 533–543, 1995.

[13] H. Ponnekanti, J. Ophir, and I. Céspedes, "Ultrasonic imaging of the stress distribution in elastic media due to an external compressor," *Ultrason. Med. Biol.*, vol. 20, no. 1, pp. 27–33, 1994.

[14] F. Kallel and M. Bertrand, "Tissue elasticity reconstruction using linear pertubation method," *IEEE Trans. Med. Imag.*, vol. 15, no. 3, pp. 299–313, 1996.

[15] M. B. Zerhouni and M. Rachedine, "Ultrasonic calibration material and method," US Patent 5,196,343, 1993.

[16] R. Croome, "Acid and alkaline hydrolysis of gelatin," *J. Appl. Chem.*, vol. 3, pp. 280–286, 1953.

[17] M. Djabourov, J.-P. Lechaire, and F. Gaill, "Structure and rheology of gelatin and collagen gels," *Biorheology*, vol. 30, nos. 3 and 4, pp. 191–205, 1993.

[18] Y. C. Fung, *A First Course in Continuum Mechanics*, 3rd ed. Englewood Cliffs, NJ: Prentice-Hall, 1994.

[19] H. Hencky, "The elastic behavior of vulcanized rubber," *Trans. Amer. Soc. Mech. Eng.*, vol. 55, no. 33, pp. 45–53, 1933.

[20] American Society for Testing and Materials, "ASTM E 111-82 Standard test method for Young's modulus, tangent modulus, and chord modulus," *Annual book of ASTM Standards* vol. 3.01, Philadelphia, PA:ASTM, 1983.

[21] W. H. Press, S. A. Teukolsky, W. T. Vettering, and B. P. Flannery, *Numerical Recipies in FORTRAN: The Art of Scientific Computing*, 2nd ed. New York: Cambridge Univ. Press, 1992.

[22] K. te Nijenhuis, "Investigation into the aging process in gels of gelatin/water systems by the measurement of their dynamic moduli. Part I—Phenomenology," *Coll. Polym. Sci.*, vol. 259, pp. 522–535, 1981.

[23] E. J. Chen, J. Novakofski, W. K. Jenkins, and J. W. D. O'Brien, "Young's modulus measurements of soft tissues with applications to elasticity imaging," *IEEE Trans. Ultrason., Ferroelect., Freq. Contr.*, vol. 43, no. 1, pp. 191–194, 1996.

Timothy J. Hall (M'88) received an A.B. in physics from the University of Michigan-Flint in 1983, and M.S. and Ph.D. degrees in medical physics from the University of Wisconsin-Madison in 1985 and 1988, respectively.

He is currently an associate professor in the Department of Radiology at The University of Kansas Medical Center. Dr. Hall's research interests include quantitative ultrasonic and elastographic imaging, and measures of observer performance and image quality.

Dr. Hall is a member of the IEEE, the Acoustical Society of America, and the American Association of Physicists in Medicine.

Mehmet Bilgen was born in Nazilli, Turkey, on December 10, 1965. He received the B.S. degree (summa cum laude) in electrical and electronics engineering from Middle East Technical University Gaziantep Campus (currently Gaziantep University), Gaziantep, Turkey, in 1987, and the M.S. and Ph.D. degrees in electrical and computer engineering and biomedical engineering from Iowa State University, Ames, IA, in 1989 and 1993, respectively.

From 1987 to 1988 he was a research and development engineer at Aselsan, Inc. while continuing his graduate study at the Middle East Technical University, Ankara, Turkey. He was a postdoctorate researcher at the Center for Nondestructive Evaluation, Ames, where he worked in inspections of materials with rough surfaces. He is currently a postdoctorate researcher in the Department of Radiology at University of Kansas Medical Center. His research interests are tissue characterization, nondestructive

evaluation, wave propagation in inhomogeneous media, and signal processing.

Dr. Bilgen is a 3-year scholarship recipient from The Scientific and Technical Research Council of Turkey.

Michael F. Insana (M'85) was born in Portsmouth, VA, on December 18, 1954. He received the B.S. degree in physics from Oakland University, Rochester, MI, in 1978 and the M.S. and Ph.D. degrees in medical physics from the University of Wisconsin, Madison, WI, in 1982 and 1983, respectively. From 1984 to 1987 he was a research physicist at the FDA's Center for Devices and Radiological Health, where he worked in medical imaging with emphasis on acoustic signal processing. He is currently Associate Professor of Radiology at the University of Kansas Medical Center.

His current research interests are acoustic imaging and tissue characterization, signal detection and estimation, observer performance measurements, and image quality assessment. He is a member of the IEEE, ASA, and AIUM professional societies.

Thomas A. Krouskop received a Bachelor of Science degree in civil engineering from Carnegie Institute of Technology in 1967, Masters of Science degree in civil engineering and biotechnology from Carnegie-Melon University in 1969, and the Doctor of Philosophy degree in biotechnology and civil engineering from Carnegie-Melon University in 1971.

Dr. Krouskop is currently a professor in the Department of Physical Medicine and Rehabilitation at the Baylor College of Medicine. In addition to this appointment, he serves as an adjunct professor in the School of Occupational Therapy at Texas Women's University, where he teaches in a master's level program in rehabilitation technology. He also holds an adjunct professorship in the Department of Mechanical Engineering and Materials Science at Rice University and at The University of Texas Dental School in the Department of Oral Biomaterials. He has been principal investigator for a National Institute on Disability and Rehabilitation Research (NIDRR) sponsored Rehabilitation Engineering Center and field initiated research projects from NIDRR. The Veterans Administration, National Research Council, NASA and private foundations have also sponsored research projects for Dr. Krouskop. He currently has research funding from government grants and industry. He has served NIDRR as a temporary director for the rehabilitation engineering center programs and has been a peer reviewer for NIDRR, VA, Paralyzed Veterans of America, and the Shriners Hospital System.

He is an active member of several professional organizations and has published extensively in the area of the effects of pressure on tissue and fitting sockets for artificial limbs. Dr. Krouskop received the Kosiak Award in 1993 for his work in pressure ulcer prevention and has served on the panels that developed the AHCPR guidelines for preventing and treating pressure ulcers. He also has received 9 United States patents.